NIH Public Access
Author Manuscript
Pediatr Pulmonol. Author manuscript; available in PMC 2013 December 01.

Published in final edited form as:
Pediatr Pulmonol. 2012 December ; 47(12): 1192–1203. doi:10.1002/ppul.22617.

THE HUMAN FETAL LUNG XENOGRAFT: VALIDATION AS MODEL OF MICROVASCULAR REMODELING IN THE POSTGLANDULAR LUNG

Monique E. De Paepe, **Sharon Chu**, **Susan Hall**, **Nicholas Heger**, **Chris Thanos**, and **Quanfu Mao**
Department of Pathology, Women and Infants Hospital, the Department of Pathology and Laboratory Medicine, Alpert Medical School of Brown University, and the Formative Center for the Evaluation of Environmental Impacts on Fetal Development, Brown University, Providence, Rhode Island

Abstract

Background—Coordinated remodeling of epithelium and vasculature is essential for normal postglandular lung development. The value of the human-to-rodent lung xenograft as model of fetal microvascular development remains poorly defined.

Aim—The aim of this study was to determine the fate of the endogenous (human-derived) microvasculature in fetal lung xenografts.

Methods—Lung tissues were obtained from spontaneous pregnancy losses (14–22 weeks' gestation) and implanted in the renal subcapsular or dorsal subcutaneous space of SCID-beige mice (T, B and NK-cell-deficient) and/or nude rats (T-cell-deficient). Informed parental consent was obtained. Lung morphogenesis, microvascular angiogenesis and epithelial differentiation were assessed at two and four weeks post-transplantation by light microscopy, immunohistochemical and gene expression studies. Archival age-matched postmortem lungs served as control.

Results—The vascular morphology, density and proliferation of renal subcapsular grafts in SCID-beige mice were similar to age-matched control lungs, with preservation of the physiologic association between epithelium and vasculature. The microvasculature of subcutaneous grafts in SCID-beige mice was underdeveloped and dysmorphic, associated with significantly lower VEGF, endoglin, and angiopoietin-2 mRNA expression than renal grafts. Grafts at both sites displayed mild airspace dysplasia. Renal subcapsular grafts in nude rats showed frequent infiltration by host lymphocytes and obliterating bronchiolitis-like changes, associated with markedly decreased endogenous angiogenesis.

Conclusion—This study demonstrates the critical importance of host and site selection to ensure optimal xenograft development. When transplanted to severely immune suppressed, NK-cell-deficient hosts and engrafted in the renal subcapsular site, the human-to-rodent fetal lung xenograft provides a valid model of postglandular microvascular lung remodeling.

Keywords

lung development; nude rat; SCID mouse; xenotransplantation; animal model

Corresponding Author: Monique E. De Paepe, M.D., Women and Infants Hospital, Dept. of Pathology, 101 Dudley Street, Providence, RI 02905, Phone: (401) 274-1122 x 1544, Fax: (401) 453-7681, mdepaepe@wihri.org.

There are no conflicts of interest for any of the authors.

$watermark-text
$watermark-text
$watermark-text

$watermark-text

$watermark-text

$watermark-text

INTRODUCTION

During fetal development, the distal lung parenchyma undergoes a series of orchestrated morphological and functional changes required for optimal postnatal gas exchange. This process is initiated *in utero* during the transition from pseudoglandular to consecutive canalicular, saccular, and early alveolar stages of lung development and, in humans, is completed after birth during the alveolar and microvascular stages [1]. Tightly coordinated architectural and cellular remodeling of the epithelial, microvascular, and supporting mesenchymal compartments results in transformation of the relatively solid pseudoglandular lung into a sponge-like alveolar lung, in which narrow septa and close apposition of vessels and lung epithelium ensure efficient gas exchange [1].

In this highly orchestrated paradigm, coordinated remodeling of the epithelial and microvascular compartments is of critical importance. A prevalent example of dysregulated pulmonary microvascular development is chronic lung disease of preterm newborns (bronchopulmonary dysplasia, BPD). In this condition, various factors associated with preterm birth and subsequent postnatal care interfere with the coordinated remodeling of the epithelial and microvascular compartments, resulting in dysmorphic microvasculature and disrupted alveolarization [2–4]. Similarly, abnormal alveolarization is observed in experimental animal models following modulation of angiogenic regulators, such as vascular endothelial growth factor (VEGF) and/or its receptor [5–8], platelet-derived growth factor alpha (PDGFα) [9], platelet endothelial cell adhesion molecule (PECAM-1) [10] and angiopoietin [11]. The intimate association between dysregulated microvascular and alveolar remodeling, seen in both clinical and experimental contexts, strongly supports the prevailing notion that normal microvascular development is a prerequisite for normal alveolar development in postglandular lungs.

The exact mechanisms whereby the various physical, chemical and genetic factors implicated in bronchopulmonary dysplasia disrupt microvascular and alveolar remodeling remain incompletely understood. *In vitro* studies, *in vivo* studies using animal models, and studies using postmortem human lung tissues [2,12] have shed some light on the pathophysiology of BPD, but are inherently limited by biological, species-specific and/or technical factors. The human fetal lung xenograft offers the possibility to maintain human fetal lungs *ex vivo* for long periods of time in optimal incubator conditions [13–17]. Furthermore, this model provides an ethically acceptable approach for experimental manipulation of human fetal lungs. The xenograft thus represents, at least in principle, a superior model with the potential to contribute significantly to our understanding of the causes and effects of dysmorphic microvascular development in BPD and other neonatal lung diseases.

Previous studies employing a rodent-to-rodent fetal lung transplant model have demonstrated that, at least in rodent allografts, the endogenous, donor-derived pulmonary microvasculature is capable of near-physiologic growth and remodeling in ectopic sites, thus faithfully replicating the capillary development of rodent lungs *in situ*[18,19]. The fate of the microvasculature in *human* fetal lung xenografts is less well known. Although the human fetal lung xenograft was developed more than 30 years ago [13], experimental emphasis in past studies has been placed on its potential value as replica of alveolar architectural maturation and epithelial cytodifferentiation, while the fate of the microvasculature has been relatively neglected [14–16]. In their study of architectural maturation and respiratory epithelial cytodifferentiation in human fetal lung xenografts, Pavlovic et al. [17] also assessed the endogenous capillary network in human-to-nude mouse renal subcapsular and subcutaneous grafts. The fetal lungs were reported to proceed through the same maturation and cytodifferentiation stages as human lungs *in situ*, albeit at an accelerated rate. However,

$watermark-text

$watermark-text

$watermark-text

there was a rapid and progressive loss of the human-derived, endogenous capillary network, resulting in severely diminished or absent graft vascularization beyond post-transplantation day 6 [17].

The value of the human fetal lung xenograft as model of physiological or pathological postglandular lung development critically depends on its capacity to replicate microvascular as well as epithelial remodeling. In this study, we formally investigated the fate of the endogenous microvasculature in the human fetal lung following transplantation to immune suppressed rodents. In concordance with others [15,17], we used both renal subcapsular and subcutaneous sites for engraftment. As graft recipients, we evaluated not only the traditionally used immune suppressed mouse, but also the nude rat, as this larger species offers several practical advantages. Our findings demonstrate that, under the appropriate experimental conditions identified in this study, the human fetal lung xenograft provides a valid model of postglandular microvascular remodeling.

MATERIALS AND METHODS

Patients

Lung samples were obtained from previable (≤ 22 weeks' gestation) second trimester stillbirths delivered at Women and Infants Hospital (Providence, RI). The study protocol was approved by the institutional review board and full informed written consent was obtained in compliance with institutional guidelines. This study was limited to fetuses delivered following spontaneous (non-induced) pregnancy loss. Fetuses delivered by elective or medical abortions and fetuses with congenital, chromosomal, pulmonary, or cardiac anomalies were excluded. In addition, fetuses with evidence of maceration, reflecting a prolonged interval between fetal demise and delivery, were excluded. Selected results obtained in xenografted lungs were compared with age-matched postmortem lungs from the archives of the Department of Pathology at Women and Infants Hospital. Fetuses with congenital, chromosomal, pulmonary, or cardiac anomalies were excluded as controls.

Harvesting of the fetal lung

The fetal examinations were performed by the Perinatal Pathology staff at Women and Infants Hospital according to standard methods. The gestational age was obtained from the records and confirmed by fetal foot length measurements. Samples for transplantation were taken from the peripheral parenchyma of the right lung. The lung tissue was cut into 1–4 mm^3 pieces under sterile conditions. The lung samples were rinsed in Hanks' Balanced Salt Solution (HBSS) and transported to the Xenotransplant Core Facility at Brown University (Providence, Rhode Island) in ice cold Leibovitz's L-15 Medium, supplemented with gentamicin (50 μg/ml), penicillin (100 U/ml) and streptomycin (100 μg/ml, all from Gibco/Invitrogen, Carlsbad, CA). The remainder of the right lung and the entire left lung were formalin-fixed, paraffin-embedded, and stained with hematoxylin and eosin for histologic analysis. The developmental stage of the preimplantation tissues was determined based on well-established morphologic criteria [1].

Fetal lung xenografts: Transplantation and processing

Transplantation was performed at the Xenotransplant Core Facility at Brown University. Recipients were six-to-twelve week-old male SCID-beige mice (Fox Chase SCID beige, Charles River, Wilmington, MA) or nude rats (Rowett nude rat, Crl:NIH-Foxn1rnu, Charles River). Animals were anesthetized with isoflurane anesthesia (Baxter Healthcare Corporation, Deerfield, IL). Two to four lung fragments (1–2 mm in greatest dimension) from each fetus were xenografted under the capsule of each kidney (2 for mice, 3–4 for rats). In addition, two to four larger lung fragments (2–3 mm in greatest dimension) were

$watermark-text

$watermark-text

$watermark-text

grafted into the dorsal subcutaneous tissue (SCID-beige mice only). All animal research was conducted in accordance with Brown University institutional guidelines for the care and use of laboratory animals in compliance with National Institute of Health guidelines.

The xenografts were analyzed two or four weeks after implantation. The animals were euthanized by an overdose of isoflurane. The grafts of one kidney were dissected free from the surrounding kidney, placed in RNA*later* (Ambion Inc., Austin, TX) and stored at −80°C for molecular analyses, as described previously [20]. The other kidney, with implants, was formalin-fixed and paraffin-embedded *in toto* for histologic and immunohistochemical studies. Similarly, a portion of the subcutaneous graft was sampled for molecular studies, while the remainder was processed for histologic studies.

Analysis of graft maturation and epithelial cytodifferentiation

Architectural maturation of the xenograft was assessed based on morphologic criteria described elsewhere [1]. Pulmonary epithelial cytodifferentiation was assessed by analysis of gene expression of surfactant protein-C (SP-C, marker of alveolar type II cells) by quantitative real-time PCR analysis. Total cellular RNA was extracted from graft homogenates using TRIzol reagent (Invitrogen, Carlsbad, CA). Total RNA (2 μg) was DNase-treated (Turbo DNA-free kit, Ambion, Austin, TX) and reverse-transcribed using the Superscript III reverse transcriptase kit (Invitrogen) according to the manufacturer's protocols. Real-time quantitative RT-PCR was performed using the TaqMan Gene Expression Master mix and the ABI 7500 Fast Real Time PCR system (Applied Biosystems, Bedford, MA) according to the manufacturer's protocols. The primer and probe sets used were obtained from Applied Biosystems: SPC (SFTPC, Hs00161628) and GAPDH (glyceraldehyde-3-phosphate dehydrogenase) (Hs02758991). The data were analyzed using the ΔΔCt method [21] and normalized to GAPDH (housekeeping gene). All samples were run in one experiment. A randomly selected "control" tissue was used as calibrator; tissue mRNA expression of remaining tissues was reported as fold change relative to the calibrator tissue. Values were averaged per experimental group.

Analysis of graft vascularization

Graft vascularization was studied by immunohistochemistry using an antibody against the endothelial marker, CD31 (PECAM-1). The antibody used in this study is specific for human (not mouse or rat) CD31 antigen (Dakocytomation Glostrup, Denmark). The vascular density of the grafts (areal fraction of air-exchanging parenchyma exhibiting CD31 immunoreactivity) was determined by computer-assisted image analysis in > 20 systematically sampled, random, non-overlapping fields using methods previously described [2,22]. The areal density of air-exchanging parenchyma (A_A[ae/lu]) was estimated by dividing the number of points falling on air-exchanging (septal) parenchyma (lung parenchyma excluding airspace) by the number of points falling on the entire field (tissue and airspace). The areal density of the CD31-immunoreactive microvascular endothelial compartment (A_A[CD31/ae]) was evaluated semiautomatically, because the immunohistochemical anti-CD31 staining of endothelial cells produced a higher optical density than that of the background parenchyma. For each section, the light intensity was standardized by threshold calibration, using CD31-negative interstitial tissue as standard. (A_A[CD31/ae]), representing the CD31-immunoreactive (endothelial) area per unit area of air-exchanging (septal) parenchyma, was determined by dividing the number of points falling on CD31-positive cells by the number of points falling on air-exchanging (septal) parenchyma, and expressed as a percentage.

Endothelial cell proliferation was assessed by double immunofluorescence studies combining labeling for Ki-67 (proliferation marker) and CD31 (endothelial cell marker), as

described before [2]. In addition, the expression of selected angiogenesis-related genes in the xenografts was studied by real-time PCR according to methods described above. The primer and probe sets used were obtained from Applied Biosystems: PECAM-1 (Hs00169777); VEGF-A (Hs00900055); endoglin (Hs00923996) and angiopoietin-2 (Hs00375822).

Data analysis

Values are expressed as mean ± standard deviation (SD). The significance of differences between groups was determined by unpaired Student *t*-test. The significance level was set at $P < 0.05$.

RESULTS

Analysis of graft morphology and maturation

Lung tissues obtained from 4 fetuses (14–17 weeks' gestation) were transplanted to kidney or subcutaneous tissue of 12 SCID-beige mice. In accordance with the gestational ages of the fetuses at the time of pregnancy loss, the preimplantation lung tissues displayed the characteristic features of pseudoglandular to early canalicular lungs. The airspaces were small, round to irregular in shape, lined by cuboidal clear epithelial cells and separated by wide, relatively cellular interstitial tissue (Fig. 1A).

Renal subcapsular grafts examined at post-transplantation week 4 showed enlargement of the airspaces and flattening of the epithelium compared with the preimplantation tissue (Fig. 1C and 1E). Although less prominent than in the original tissue, the interstitium remained relatively wide and cellular. Occasional epithelial projections from the wall were noted, resulting in an irregular "pseudo-saccular" appearance of the airspace contours (Fig. 1C). The grafts were separated from the underlying renal cortex by a very thin layer of fibrous connective tissue and, in some areas, lung epithelium appeared to abut directly the renal cortical tubules (Fig. 1C). Inflammatory cells were absent from the graft-kidney interface. According to standard morphologic criteria, the appearance of the xenografts at this stage, characterized by airspace dilation, epithelial flattening and occasional presence of blunt epithelial projections, is most consistent with early saccular stage of development. However, the airspaces appeared more dilated and rounded than expected for age-matched early saccular lungs developed *in situ* (Fig. 1B).

Following implantation of 3–4 individual lung samples, subcutaneous grafts coalesced into a single well-circumscribed mass. This graft conglomerate was encapsulated by a relatively thick layer of fibroconnective tissue, which clearly separated the grafts from the surrounding subcutaneous soft tissue (Fig. 1D and 1F). Focal scarring was occasionally noted (Fig. 1F). The architectural development of the subcutaneous grafts appeared less homogeneous than that of the renal grafts. The center of the grafts contained areas with small- to medium-sized airspaces of uniform size, separated by relatively wide septa similar to the appearance of renal grafts. However, in most areas, the lung tissue showed more dilated and simplified airspaces, separated by thin intervening septa (Fig. 1D and 1F). Airspace dilation and septal thinning was especially prominent at the periphery of the grafts (Fig. 1D). Thin septal projections were noted (Fig. 1D). There was no evidence of inflammation associated with the grafts.

Alveolar epithelial cytodifferentiation in grafts was estimated by real-time PCR analysis of SP-C mRNA expression. At post-transplantation week 2, SP-C mRNA levels were significantly higher in renal graft homogenates than in subcutaneous grafts (Fig. 2). SP-C mRNA levels were significantly higher at 4 weeks than at 2 weeks at both implantation sites, suggestive of ongoing maturation and epithelial cytodifferentiation. By post-transplantation week 4, SP-C mRNA expression was equally high in renal and subcutaneous

$watermark-text $watermark-text $watermark-text

grafts, suggestive of “catch-up” epithelial growth and differentiation in subcutaneous grafts (Fig. 2).

Analysis of graft vascularization

Endogenous (human-derived) graft vascularization was studied by immunohistochemical analysis using a human CD31-specific antibody that does not cross-react with murine or rat endothelial cells. Renal subcapsular grafts studied at post-transplant week 4 showed a well-developed capillary network, diffusely present throughout the entire graft with extension from the graft into the subjacent murine renal cortex (Fig. 3A). The graft microvasculature was organized in a sheetlike near-continuous single or double-track pattern within the septa. The capillary profiles closely followed the outline of the airspaces and were usually situated immediately beneath the epithelium (Fig. 3D).

Compared with renal grafts, subcutaneous grafts displayed less abundant and less evenly distributed human CD31-positive capillaries (Fig. 3B and 3E). Rather than forming continuous linear arrays tracing the septal outlines, the vasculature of subcutaneous grafts was visualized as short, interrupted CD31-positive profiles, more haphazardly arranged within the septa (Fig. 3B and 3E). Rare vascular extensions into the surrounding fibroconnective capsule were present, never reaching beyond the capsule into the subcutaneous soft tissue (Fig. 3B, asterisk).

As a reference, we studied the microvascular morphology in representative human lungs at 21 weeks’ gestation, corresponding to the corrected age of 17-week xenografts at 4 weeks post-transplantation. While the CD31 staining appeared more intense, the pattern and location of the microvasculature in control lungs were similar to those of renal subcapsular xenografts (Fig. 3C and 3F). Both in control lungs and renal xenografts, the capillaries were arranged as a dense single or double capillary network in close subepithelial apposition.

We further evaluated the proliferative activity of endothelial cells at 4 weeks post-transplantation by double immunofluorescence studies combining CD31 and Ki-67 labeling. Proliferation was readily visualized in CD31-positive endothelial cells in renal subcapsular grafts (Fig. 3G) and in age-matched 21-week gestation control lungs (Fig. 3I), confirming that endogenous, human-derived endothelial cells are capable of brisk proliferation up to at least 4 weeks post-transplantation. Proliferation was overall less frequent in the more sparse vessels present in subcutaneous grafts, although occasional endothelial proliferative activity was noted (Fig. 3H).

The qualitative impression of increased vascularization in renal subcapsular grafts compared with subcutaneous grafts was confirmed by morphometric assessment of the vascular density (ratio of CD31-positive area over total area of air-exchanging parenchyma, expressed as a percentage). The vascular density was significantly more than two-fold higher in renal subcapsular grafts than in subcutaneous grafts, both at two and four weeks post-transplantation (Fig. 4). Moreover, the vascular density of renal grafts was equivalent to that of age-matched control lungs (Fig. 4).

The areal density of air-exchanging (septal) parenchyma (A_A[ae/lu]), representing the fraction of distal lung parenchyma comprised of septal tissue, rather than airspace, tended to be larger in renal subcapsular grafts than in subcutaneous grafts (55.2 ± 1.4% versus 49.2 ± 3.9%, $P = 0.052$). The qualitative impression of increased vascularization in renal subcapsular grafts compared with subcutaneous grafts was confirmed by morphometric assessment of the areal density of the CD31-immunoreactive microvascular endothelial compartment (A_A[CD31/ae]) (ratio of CD31-positive area over area of air-exchanging parenchyma, expressed as a percentage) or vascular density. The vascular density was

$watermark-text $watermark-text $watermark-text

$watermark-text

$watermark-text

$watermark-text

significantly more than two-fold higher in renal subcapsular grafts than in subcutaneous grafts, both at two and four weeks post-transplantation (Fig. 4). Moreover, the vascular density of renal grafts was equivalent to that of age-matched control lungs (Fig. 4).

Analysis of angiogenesis-related gene expression in xenografts

The CD31 immunohistochemical studies indicated that graft vascularization by endogenous, human-derived vessels, was more robust in renal subcapsular grafts than in subcutaneous grafts. To further investigate this correlation, we determined the mRNA levels of this endothelial marker (CD31, PECAM-1) in both graft types by real-time RT-PCR. In accordance with the morphologic and morphometric analyses, we determined that the mRNA levels of PECAM-1/CD31 were significantly higher in renal than subcutaneous grafts (Fig. 5A). At both sites, the PECAM-1 mRNA levels were similar at 2 and 4 weeks post-transplantation.

To begin to understand the mechanisms contributing to the observed site-specific differences in vascularization, we compared the expression levels of key regulators of postglandular angiogenesis in grafts at both sites. As shown, the mRNA levels of VEGFA, endoglin and angiopoietin-2 were significantly higher in renal subcapsular grafts than in subcutaneous grafts, both at two and four weeks post-transplantation (Fig. 5B–D).

Analysis of xenograft outcome in the nude rat host

In a separate set of experiments, we assessed the value of the nude (RNU) rat as recipient of renal subcapsular grafts. A major advantage of this species is its larger size and greater tolerance of surgical procedures. Lung tissues from 11 fetuses (14–22 weeks' gestation) were transplanted to 33 nude rats. As anticipated, the rat kidney easily supported up to three or four individual grafts per organ (i.e. 8 grafts per animal).

In contrast with similar grafts in murine SCID-beige recipients, renal subcapsular grafts in the nude rat host displayed a high frequency of inflammation. Although often subtle at this time point, inflammatory infiltrates were detected in 37/56 (66%) grafts and 17/19 (89%) animals at post-transplantation week 2. By post-transplantation week 4, 36/38 (95%) grafts and all 14 animals studied showed moderate to marked degrees of host-versus-graft inflammatory response. The inflammation was most prominent along the graft-kidney interface, where it formed a band-like cellular sheet of varying thickness (Fig. 6A). In some grafts, inflammation involved only part of the graft-kidney interface (Fig. 6B). Interestingly, in such grafts with only partial inflammatory involvement, endogenous capillaries tended to be absent or markedly diminished in the portion of the graft overlying the inflammatory infiltrates, whereas the part of the graft with less or no inflammation showed unperturbed endogenous vascularization (Fig. 6B–C). The inflammatory infiltrates failed to stain with anti-human CD45 (leukocyte common antigen) antibody, confirming their non-human (rat) origin (not shown).

In addition to linear inflammatory aggregates along the graft-kidney interface, 18/38 (47%) grafts at post-transplantation week 4 displayed prominent inflammation deep within the graft, associated with peribronchial inflammation and inflammatory fibroproliferative plugging involving small- and medium-sized bronchi (Fig. 6D–E). These pathologic findings involving the bronchioles were strongly reminiscent of obliterative bronchiolitis, as seen in the context of human lung transplant rejection. Graft vascularization was markedly diminished in such heavily inflamed areas (Fig. 6F). In some cases, graft inflammation resulted in complete obliteration of the lung parenchyma, leaving only a nodular subcapsular lymphoid aggregate (not shown).

$watermark-text

$watermark-text

$watermark-text

DISCUSSION

In this study, we determined the value of the human-to-rodent fetal lung xenograft as model of physiological postglandular lung development, with special emphasis on the remodeling of the endogenous (human-derived) microvasculature. We first assessed the potential importance of the anatomic engraftment site as determinant of the outcome of the xenotransplantation, focusing on renal subcapsular and subcutaneous locations as most frequently reported implantation sites. Using a combination of morphological, immunohistochemical, and molecular techniques to monitor the fate of vessels and endothelial cells, we determined that the vascular morphology, the vascular density, and the relationship of the vasculature to the epithelium in renal subcapsular xenografts were similar to those of age-matched control lungs. We further determined that this vascular remodeling occurred in synchrony with architectural and cellular remodeling of the respiratory epithelium, as evidenced by widening of the airspaces, flattening of the lining epithelium, and increased surfactant protein-C expression.

The exact mode(s) of angiogenesis in the renal subcapsular grafts remain to be determined. Angiogenesis is defined as the formation of new blood vessels from pre-existing ones. Several different modes and mechanisms exist [23,24], but endothelial sprouting [25,26] and intussusceptive angiogenesis [27–29] have received most attention. Endothelial sprouting involves sequential basement membrane degradation, endothelial cell proliferation, formation of solid sprouts composed of endothelial cells, remodeling of the sprout with creation of a lumen, and final integration into the vascular network [25]. Non-sprouting angiogenesis by intussusception was first recognized in the lung as a means of capillary network growth and remodeling [30,31]. Intussusceptive angiogenesis involves growth and remodeling of a microvascular system based on partitioning of the vessel lumen by insertion of connective tissue columns, called tissue pillars or posts, into the lumen [27–29].

The present morphologic studies do not allow definitive elucidation of the mechanisms of angiogenesis in the renal subcapsular human lung xenografts, as detection of pillar formation, for instance, requires detailed three-dimensional imaging analyses [29]. Certain features of the xenograft vasculature, including the presence of a sheet-like vascular network within the septa with occasional sinusoidal dilatations, are suggestive of intussusceptive microvascular remodeling. In contrast, the slender, monopodial graft-derived vessels at the graft-kidney interface may represent sprouting angiogenesis. Similar zone-dependent combinations of sprouting and intussusceptive angiogenesis have been described in tumor xenograft models [32] and in post-pneumonectomy lung growth [33].

Whereas the endogenous microvasculature in renal subcapsular grafts faithfully replicated the highly orchestrated remodeling characteristic of human postglandular lungs *in situ*, microvascular remodeling was significantly more uneven in the subcutaneous implantation site where the microvasculature was dysmorphic and significantly underdeveloped. To gain insight into the mechanisms underlying the disparate vascular growth in renal and subcutaneous sites, we studied the expression levels of selected angiogenic regulators in the respective graft lysates. Corresponding to decreased vascular growth in subcutaneous grafts, the mRNA levels of VEGFA, endoglin, and angiopoietin-2 were found to be significantly lower in subcutaneous grafts than in renal grafts, suggesting the observed differential vascular growth at these sites may be mediated, in part, by differential expression of these angiogenic regulators.

Others have previously demonstrated that vascular perfusion of the xenograft is established by the formation of connections between graft and host capillary networks [19]. As we determined in this study, subcutaneous grafts are encapsulated by a relatively thick layer of

$watermark-text

$watermark-text

$watermark-text

fibroconnective tissue that clearly separates the coalesced grafts from the surrounding fibroadipose tissue. In contrast, renal grafts are intimately connected to the underlying renal cortex and, in fact, human-derived vessels extended from the graft into the underlying renal cortex in all cases. We therefore speculate that the fibrous capsule surrounding the subcutaneous grafts may create a physical barrier that prevents or disrupts the formation of vascular anastomoses between graft and host vasculature, thus contributing to underdevelopment of the graft vasculature.

In addition to implantation site, we assessed the potential importance of host selection on graft outcome. In this study, we used immune suppressed strains of two different rodent species as graft recipients: SCID-beige mice and nude rats. The congenic SCID-beige mouse possesses two autosomal recessive mutations: SCID ($Prkdc^{scid}$) and beige ($Lyst^{bg}$). The SCID mutation results in severe combined immunodeficiency affecting both the B and T lymphocytes, while the beige mutation results in defective natural killer (NK) cells [34]. In contrast to SCID-beige mice, the athymic RNU rat is T cell-deficient only [35]. The main rationale for inclusion of the nude rat was its larger size, which offers several practical advantages for *in vivo* experimentation, including greater tolerance of surgical procedures and repeated blood sampling, and accommodation of a larger number of grafts.

The vast majority of renal xenografts in nude rats displayed evidence of immunologic rejection by post-transplantation week 4, as evidenced by the build-up of host-derived inflammatory aggregates along the graft-host interface. Similar inflammatory infiltrates were not seen in grafts transplanted to SCID-beige mice. Although species-specific factors may contribute, we suspect that the observed inflammatory response may be linked to the greater immune competence of nude rats, in particular the presence of host-derived NK cells, which are present in nude rats but absent or deficient in SCID-beige mice [34,35]. Interestingly, host-derived inflammation appeared to adversely impact graft vascularization, presumably by interfering with the formation of connections between graft and host vessels in the affected region. Of note, others previously described similar evidence of immunologic rejection in non-irradiated nude rats following orthotopic implantation of lung cancer cells [36]. In that study, pretreatment of the animals with gamma irradiation prevented rejection, suggesting additional immunosuppression might attenuate or prevent the observed rejection in the human fetal lung xenograft context as well.

The host-versus-graft inflammatory response in nude rats was usually limited to a band-like aggregate of host-derived mononuclear cells at the interface between graft and host kidney. In some cases, however, multifocal inflammatory infiltrates extended deep within the graft, associated with occlusion of small airways by vascularized fibrous tissue. These findings reproduced the characteristic features of obliterative bronchiolitis (OB), an inflammatory and fibroproliferative small airway disorder that remains a major limitation to the long-term success of human lung transplantation [37,38]. Several animal models have been developed to elucidate the complex pathophysiology of this condition, including ortho- or heterotopic lung and trachea transplantation in rodents and large animals based on mismatched lung allografts (e.g. between genetically discordant rat strains) (reviewed in [39]). To our knowledge, the obliterative bronchiolitis-like fibroproliferative and inflammatory reaction seen in human fetal lung xenografts in the present study may represent the first reported human lung-based experimental model of this disease.

In our study, renal subcapsular grafts displayed consistently high levels of graft vascularization, replicating the vascular density and patterns of age-matched control lungs. In contrast, Pavlovic et al. [17] recently described rapid and progressive loss of endogenous capillaries in both renal subcapsular and subcutaneous human fetal lung xenografts. While the reasons for these discrepant findings are not clear, it is possible that the type of immune

$watermark-text

$watermark-text

$watermark-text

suppressed mouse strain used as xenograft recipient may have contributed to these disparate results. Whereas we used T, B, and NK cell-deficient SCID-beige mice, Pavlovic et al. used T-cell deficient athymic outbred NCr nude mice (CrTac:NCr-*Foxn1*^{nu}) as recipients [17]. As we have demonstrated in this study, host-versus-graft immune responses, such as seen in nude rats, may interfere with endogenous microvascular development. It is therefore possible that the enhanced immune suppression of SCID-beige mouse compared with the NCr nude mouse may explain, in part, the greater microvascular development observed in xenografts in our model.

Our study identified profoundly immune compromised mice such as SCID-beige mice as optimal for lung xenograft studies. While SCID-beige mice did not display evidence of graft rejection in this study, it needs to be emphasized that this animal strain has its own specific limitations. In particular, SCID mice and their derivatives are susceptible to the development of spontaneous T-cell lymphoma, which reportedly occurs in 15–20% of SCID mice and as early as 10 weeks of age [40,41]. In a separate set of studies not included in the present report, we performed human fetal lung transplantation in a small cohort of older SCID-beige mice (10–12 weeks at time of engraftment). Interestingly, in one animal that developed widespread T-cell lymphoma in most thoracic and abdominal viscera, tumor cells were found to infiltrate the renal and subcutaneous lung xenografts as well (not shown). As the presence of tumor infiltrates will obviously interfere with most experiments involving lung xenografts, it may be prudent to consider this age-specific tumor risk of the SCID-derived hosts in the study design.

In conclusion, we have determined the strengths and limitations of the human fetal lung xenograft, focusing on its value as model of postglandular microvascular remodeling. We established that human fetal lung xenografts can serve as a valid model of postglandular lung remodeling with faithful retention of the epithelial-vascular interrelationships. The value of the xenograft as a physiologic model is enhanced by use of more profoundly immune suppressed rodent hosts, such as T, B, and NK-cell-deficient SCID-beige mice, and by use of the renal subcapsular, rather than subcutaneous location, as engraftment site. Under these conditions, the xenograft approach provides an invaluable strategy for studies evaluating the pathophysiology of neonatal lung diseases, especially those characterized by dysmorphic microvascular development. In addition, this model may be of great value for studies focused on the developmental effects of pharmacologic or environmental toxicants on postglandular lungs.

Acknowledgments

These studies were performed under the auspices of the NIH P20 Formative Center for the Evaluation of Environmental Impacts on Fetal Development at Brown University (PI: Dr. Kim Boekelheide). Consent was obtained by the staff of the Tissue Procurement Core of the Formative Center (PI: Dr. Maureen Phipps) and transplantation was performed by the staff of the Xenograft Core (PI: Dr. Chris Thanos). We are grateful to the parents who gave their consent for these studies. The contributions of Terese Pasquariello, M.S. and Virginia Hovenasian to the immunohistochemistry studies and to the immunofluorescence imaging studies, respectively, are gratefully acknowledged.

Supported in part by NIH P20 ES018169 Formative Center for the Evaluation of Environmental Impacts on Fetal Development (MEDP, CT)

REFERENCES

1. De Paepe, ME. Lung growth and development. In: Churg, AM.; Myers, JL.; Tazelaar, HD.; Wright, JL., editors. Thurlbeck's pathology of the lung. New York: Thieme Medical Publishers; 2005.

$watermark-text
$watermark-text
$watermark-text

2. De Paepe ME, Mao Q, Powell J, Rubin SE, DeKoninck P, Appel N, Dixon M, Gundogan F. Growth of pulmonary microvasculature in ventilated preterm infants. Am J Respir Crit Care Med. 2006; 173:204–211. [PubMed: 16210670]
3. Thebaud B, Abman SH. Bronchopulmonary dysplasia: where have all the vessels gone? Roles of angiogenic growth factors in chronic lung disease. Am J Respir Crit Care Med. 2007; 175:978–985. [PubMed: 17272782]
4. Abman SH. Bronchopulmonary dysplasia: "a vascular hypothesis". Am J Respir Crit Care Med. 2001; 164:1755–1756. [PubMed: 11734417]
5. Kasahara Y, Tuder RM, Taraseviciene-Stewart L, Le Cras TD, Abman S, Hirth PK, Waltenberger J, Voelkel NF. Inhibition of VEGF receptors causes lung cell apoptosis and emphysema. J Clin Invest. 2000; 106:1311–1319. [PubMed: 11104784]
6. Le Cras TD, Spitzmiller RE, Albertine KH, Greenberg JM, Whitsett JA, Akeson AL. VEGF causes pulmonary hemorrhage, hemosiderosis, and air space enlargement in neonatal mice. Am J Physiol Lung Cell Mol Physiol. 2004; 287:L134–L142. [PubMed: 15033636]
7. Le Cras TD, Markham NE, Tuder RM, Voelkel NF, Abman SH. Treatment of newborn rats with a VEGF receptor inhibitor causes pulmonary hypertension and abnormal lung structure. Am J Physiol Lung Cell Mol Physiol. 2002; 283:L555–L562. [PubMed: 12169575]
8. McGrath-Morrow SA, Cho C, Zhen L, Hicklin DJ, Tuder RM. Vascular endothelial growth factor receptor 2 blockade disrupts postnatal lung development. Am J Respir Cell Mol Biol. 2005; 32:420–427. [PubMed: 15722510]
9. Bostrom H, Willetts K, Pekny M, Leveen P, Lindahl P, Hedstrand H, Pekna M, Hellstrom M, Gebre-Medhin S, Schalling M, Nilsson M, Kurland S, Tornell J, Heath JK, Betsholtz C. PDGF-A signaling is a critical event in lung alveolar myofibroblast development and alveogenesis. Cell. 1996; 85:863–873. [PubMed: 8681381]
10. DeLisser HM, Helmke BP, Cao G, Egan PM, Taichman D, Fehrenbach M, Zaman A, Cui Z, Mohan GS, Baldwin HS, Davies PF, Savani RC. Loss of PECAM-1 function impairs alveolarization. J Biol Chem. 2006; 281:8724–8731. [PubMed: 16377626]
11. Hato T, Kimura Y, Morisada T, Koh GY, Miyata K, Tabata M, Kadomatsu T, Endo M, Urano T, Arai F, Araki K, Suda T, Kobayashi K, Oike Y. Angiopoietins contribute to lung development by regulating pulmonary vascular network formation. Biochem Biophys Res Commun. 2009; 381:218–223. [PubMed: 19217887]
12. De Paepe ME, Patel C, Tsai A, Gundavarapu S, Mao Q. Endoglin (CD105) up-regulation in pulmonary microvasculature of ventilated preterm infants. Am J Respir Crit Care Med. 2008; 178:180–187. [PubMed: 18420967]
13. Cobb LM. Growth and development of human fetal trachea and lung in immune-deprived mice. Thorax. 1975; 30:357–359. [PubMed: 1096353]
14. Berin MC, Eckmann L, Broide DH, Kagnoff MF. Regulated production of the T helper 2-type T-cell chemoattractant TARC by human bronchial epithelial cells in vitro and in human lung xenografts. Am J Respir Cell Mol Biol. 2001; 24:382–389. [PubMed: 11306430]
15. Peault B, Tirouvanziam R, Sombardier MN, Chen S, Perricaudet M, Gaillard D. Gene transfer to human fetal pulmonary tissue developed in immunodeficient SCID mice. Hum Gene Ther. 1994; 5:1131–1137. [PubMed: 7530495]
16. Groscurth P, Tondury G. Cytodifferentiation of human fetal lung tissue following transplantation into "nude" mice. Anat Embryol (Berl). 1982; 165:291–302. [PubMed: 6760745]
17. Pavlovic J, Floros J, Phelps DS, Wigdahl B, Welsh P, Weisz J, Shearer DA, Leure du Pree A, Myers R, Howett MK. Differentiation of xenografted human fetal lung parenchyma. Early Hum Dev. 2008; 84:181–193. [PubMed: 17555893]
18. Schwarz MA, Zhang F, Lane JE, Schachtner S, Jin Y, Deutsch G, Starnes V, Pitt BR. Angiogenesis and morphogenesis of murine fetal distal lung in an allograft model. Am J Physiol Lung Cell Mol Physiol. 2000; 278:L1000–L1007. [PubMed: 10781431]
19. Vu TH, Alemayehu Y, Werb Z. New insights into saccular development and vascular formation in lung allografts under the renal capsule. Mech Dev. 2003; 120:305–313. [PubMed: 12591600]
20. De Paepe ME, Mao Q, Huang C, Zhu D, Jackson CL, Hansen K. Postmortem RNA and protein stability in perinatal human lungs. Diagn Mol Pathol. 2002; 11:170–176. [PubMed: 12218457]

$watermark-text
$watermark-text
$watermark-text

21. Livak KJ, Schmittgen TD. Analysis of relative gene expression data using real-time quantitative PCR and the 2(-Delta Delta C(T)) Method. Methods. 2001; 25:402–408. [PubMed: 11846609]
22. De Paepe ME, Johnson BD, Papadakis K, Sueishi K, Luks FI. Temporal pattern of accelerated lung growth after tracheal occlusion in the fetal rabbit. Am J Pathol. 1998; 152:179–190. [PubMed: 9422535]
23. Dome B, Hendrix MJ, Paku S, Tovari J, Timar J. Alternative vascularization mechanisms in cancer: Pathology and therapeutic implications. Am J Pathol. 2007; 170:1–15. [PubMed: 17200177]
24. Augustin HG. Tubes, branches, and pillars: the many ways of forming a new vasculature. Circ Res. 2001; 89:645–647. [PubMed: 11597985]
25. Paku S, Paweletz N. First steps of tumor-related angiogenesis. Lab Invest. 1991; 65:334–346. [PubMed: 1716330]
26. van Hinsbergh VW, Koolwijk P. Endothelial sprouting and angiogenesis: matrix metalloproteinases in the lead. Cardiovasc Res. 2008; 78:203–212. [PubMed: 18079100]
27. Makanya AN, Hlushchuk R, Djonov VG. Intussusceptive angiogenesis and its role in vascular morphogenesis, patterning, and remodeling. Angiogenesis. 2009; 12:113–123. [PubMed: 19194777]
28. Djonov V, Baum O, Burri PH. Vascular remodeling by intussusceptive angiogenesis. Cell Tissue Res. 2003; 314:107–117. [PubMed: 14574551]
29. Burri PH, Hlushchuk R, Djonov V. Intussusceptive angiogenesis: its emergence, its characteristics, and its significance. Dev Dyn. 2004; 231:474–488. [PubMed: 15376313]
30. Caduff JH, Fischer LC, Burri PH. Scanning electron microscope study of the developing microvasculature in the postnatal rat lung. Anat Rec. 1986; 216:154–164. [PubMed: 3777448]
31. Burri PH, Tarek MR. A novel mechanism of capillary growth in the rat pulmonary microcirculation. Anat Rec. 1990; 228:35–45. [PubMed: 2240600]
32. Djonov V, Andres AC, Ziemiecki A. Vascular remodelling during the normal and malignant life cycle of the mammary gland. Microsc Res Tech. 2001; 52:182–189. [PubMed: 11169866]
33. Konerding MA, Gibney BC, Houdek JP, Chamoto K, Ackermann M, Lee GS, Lin M, Tsuda A, Mentzer SJ. Spatial dependence of alveolar angiogenesis in post-pneumonectomy lung growth. Angiogenesis. 2012; 15:23–32. [PubMed: 21969134]
34. MacDougall JR, Croy BA, Chapeau C, Clark DA. Demonstration of a splenic cytotoxic effector cell in mice of genotype SCID/SCID.BG/BG. Cell Immunol. 1990; 130:106–117. [PubMed: 2144467]
35. Cash JM, Remmers EF, Goldmuntz EA, Crofford LJ, Zha H, Hansen CT, Wilder RL. Genetic mapping of the athymic nude (RNU) locus in the rat to a region on chromosome 10. Mamm Genome. 1993; 4:37–42. [PubMed: 8422500]
36. Howard RB, Chu H, Zeligman BE, Marcell T, Bunn PA, McLemore TL, Mulvin DW, Cowen ME, Johnston MR. Irradiated nude rat model for orthotopic human lung cancers. Cancer Res. 1991; 51:3274–3280. [PubMed: 2040002]
37. Trulock EP, Christie JD, Edwards LB, Boucek MM, Aurora P, Taylor DO, Dobbels F, Rahmel AO, Keck BM, Hertz MI. Registry of the International Society for Heart and Lung Transplantation: twenty-fourth official adult lung and heart-lung transplantation report-2007. J Heart Lung Transplant. 2007; 26:782–795. [PubMed: 17692782]
38. Sato M, Keshavjee S. Bronchiolitis obliterans syndrome: alloimmune-dependent and -independent injury with aberrant tissue remodeling. Semin Thorac Cardiovasc Surg. 2008; 20:173–182. [PubMed: 18707652]
39. Sato M, Keshavjee S, Liu M. Translational research: animal models of obliterative bronchiolitis after lung transplantation. Am J Transplant. 2009; 9:1981–1987. [PubMed: 19663891]
40. Custer RP, Bosma GC, Bosma MJ. Severe combined immunodeficiency (SCID) in the mouse. Pathology, reconstitution, neoplasms. Am J Pathol. 1985; 120:464–477. [PubMed: 2412448]
41. Nishimura M, Wakana S, Kakinuma S, Mita K, Ishii H, Kobayashi S, Ogiu T, Sado T, Shimada Y. Low frequency of Ras gene mutation in spontaneous and gamma-ray-induced thymic lymphomas of scid mice. Radiat Res. 1999; 151:142–149. [PubMed: 9952298]

$watermark-text
$watermark-text
$watermark-text

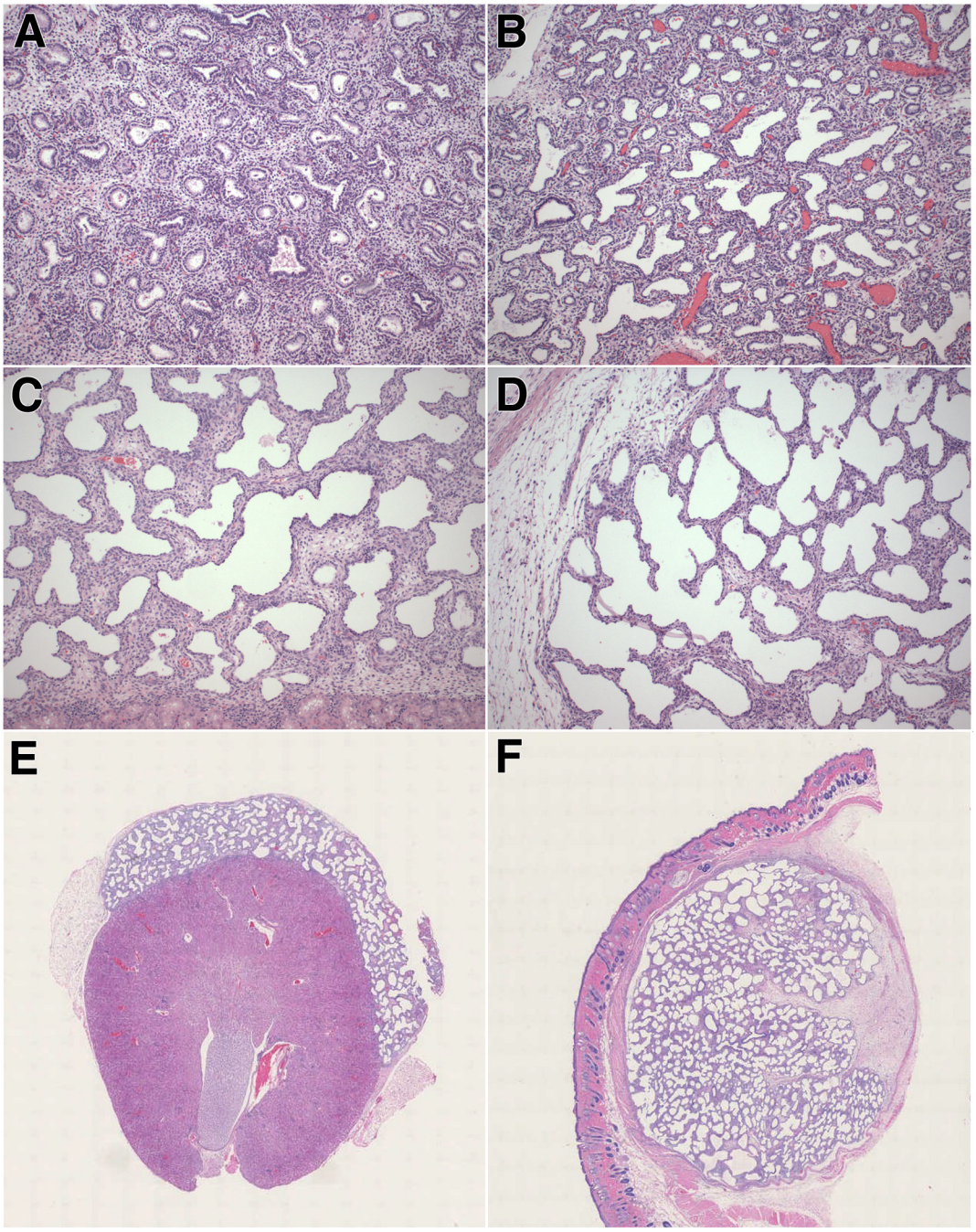

Figure 1. Morphology of preimplantation lung, control lung and xenografts

A. Representative preimplantation lung at 17 weeks' gestation (pseudoglandular - early canalicular stage of development).

B. Representative control lung at 21 weeks' gestation (canalicular stage).

C–D. Representative photomicrographs of renal subcapsular (C) and subcutaneous (D) xenografts, obtained at 17 weeks' gestation and studied at post-transplantation week 4.

E–F Scanned images of representative renal subcapsular (E) and subcutaneous (F) xenografts, obtained at 17 weeks' gestation and studied at post-transplantation week 4.

A–F: Hematoxylin-eosin stain. A–D: original magnification X100; E and F: original magnification X5.

$watermark-text
$watermark-text
$watermark-text

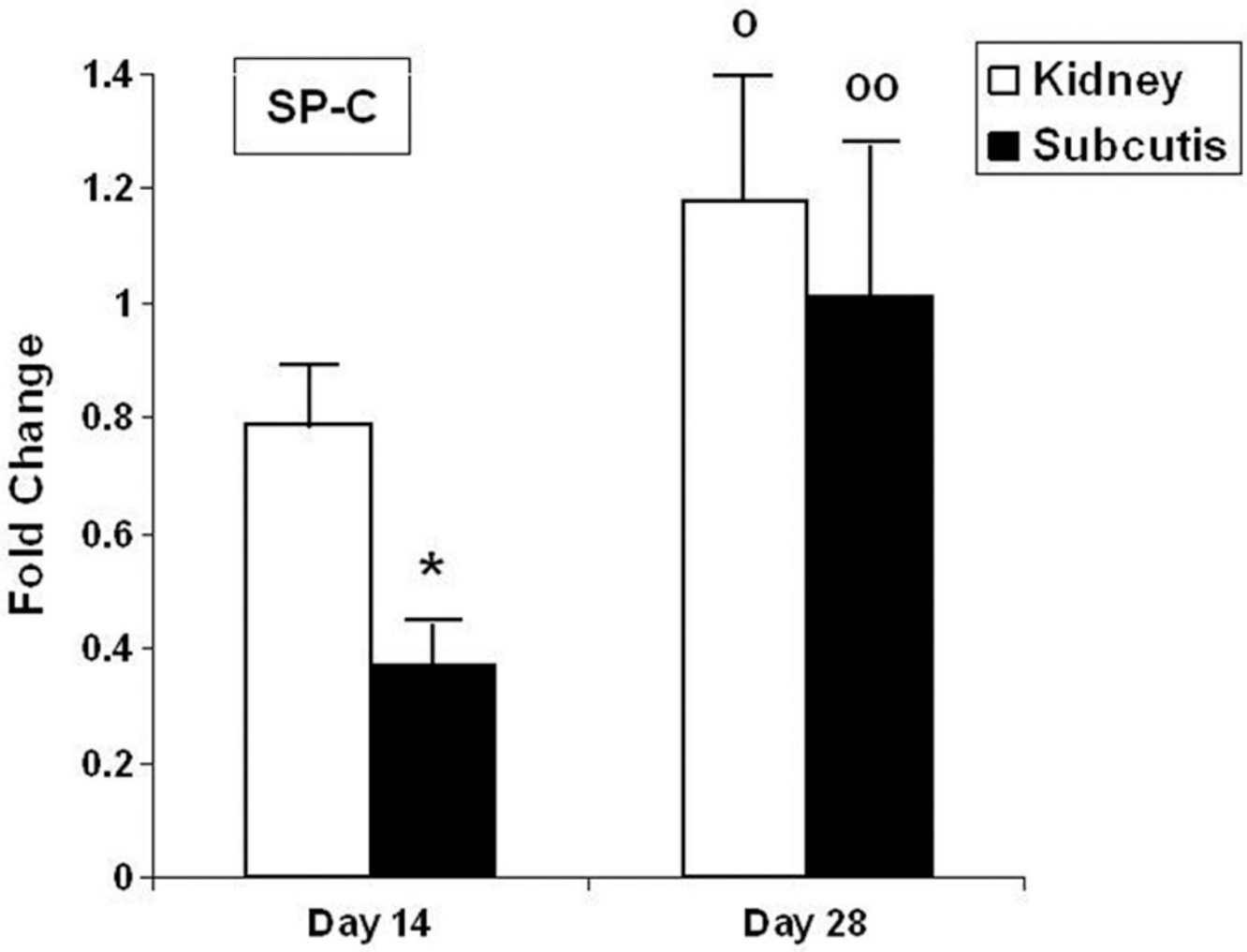

Figure 2. Analysis of surfactant protein-C gene expression in grafts

Values represent mean ± SD of 4–6 animals per group, normalized to GAPDH expression.

Open bars: kidney grafts; closed bars: subcutaneous grafts.

SP-C: surfactant protein-C

*: $P < 0.001$ versus kidney graft; °: $P < 0.05$; °°: $P < 0.01$ versus day 14.

$watermark-text
$watermark-text
$watermark-text

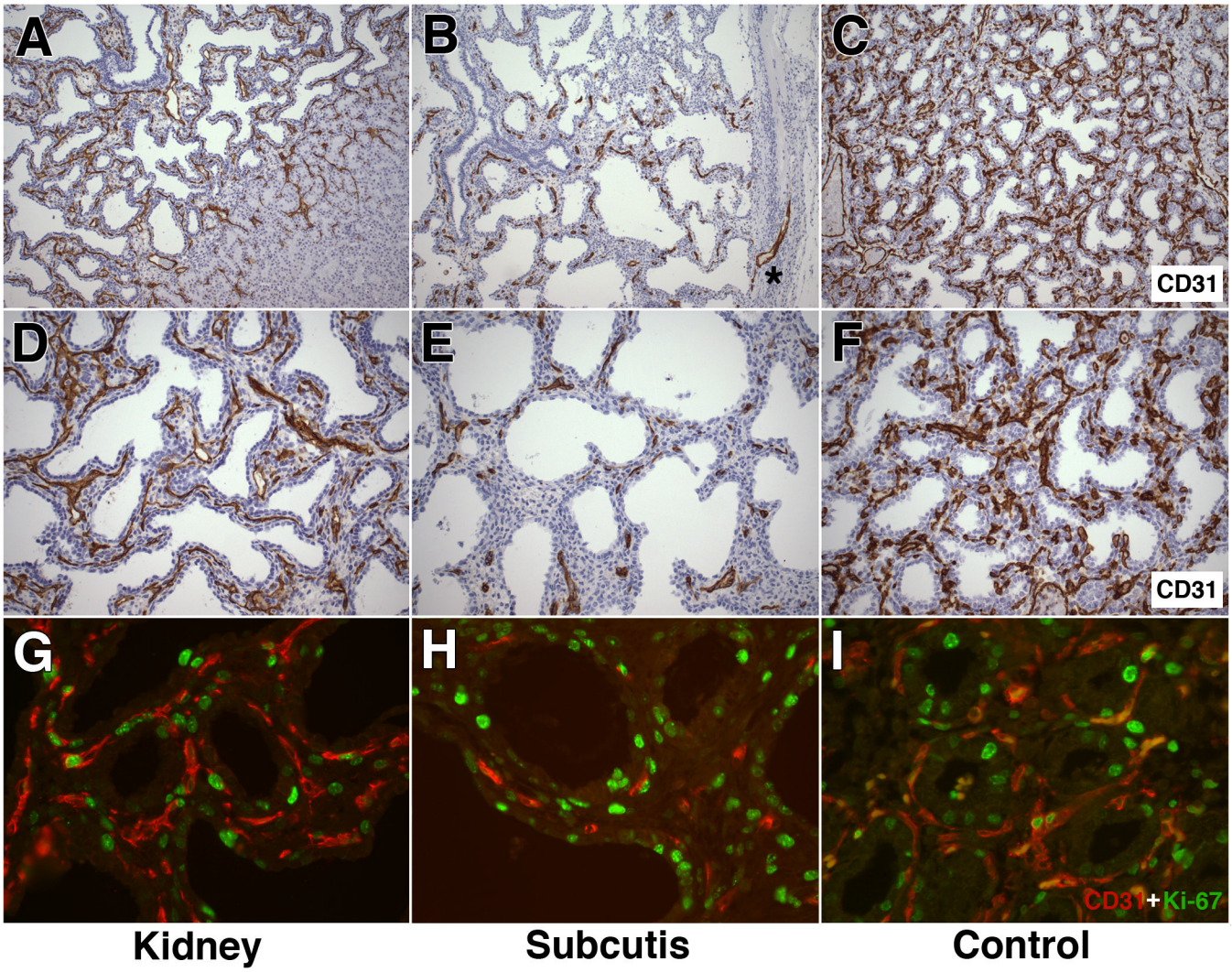

Figure 3. Analysis of graft vascularization and endothelial cell proliferation

A and D: Representative CD31-immunohistochemical analysis of renal subcapsular xenografts (obtained at 17 weeks' gestation, studied at post-transplant week 4). A dense capillary network is noted within the septa, forming a near-continuous single or double capillary pattern in subepithelial position. Graft-derived capillaries extend deep into adjacent murine renal cortex (Fig. 3A, right).

B and E: Representative CD31-immunohistochemical analysis of subcutaneous xenografts (obtained at 17 weeks' gestation, studied at post-transplant week 4). Graft capillaries are seen as short, interrupted profiles within the septa. Some areas appear devoid of vessels (Fig. 3B, top). Rare vascular extension from graft into surrounding fibrous capsule is noted (Fig. 3B, asterisk). Airspaces appear dilated.

C and F: Representative control lung at 21 weeks' gestation showing an intensely CD31-immunoreactive capillary network, organized as a single or double network below the epithelium.

G: Representative renal subcapsular graft at post-transplant week 4 showing a well developed capillary network with numerous proliferating endothelial cells, exhibiting double immunoreactivity for Ki-67 (green, nuclear) and CD31 (red, cytoplasmic).

H. Representative subcutaneous graft at post-transplant week 4 showing focal presence of septal capillaries. Only rare endothelial proliferative activity is seen.

I. Representative control lung at 21 weeks' gestation showing proliferating endothelial cells in a dense capillary network.

A–F: CD-31 (PECAM-1) immunohistochemical analysis (DAB-peroxidase staining with hematoxylin counterstain). A–C: original magnification: X100; D–F: original magnification: X200.

G–I: Ki-67 (Alexafluor-green) and CD31 (Cy3-red) double immunofluorescence; original magnification: X400).

$watermark-text
$watermark-text
$watermark-text

$watermark-text
$watermark-text
$watermark-text

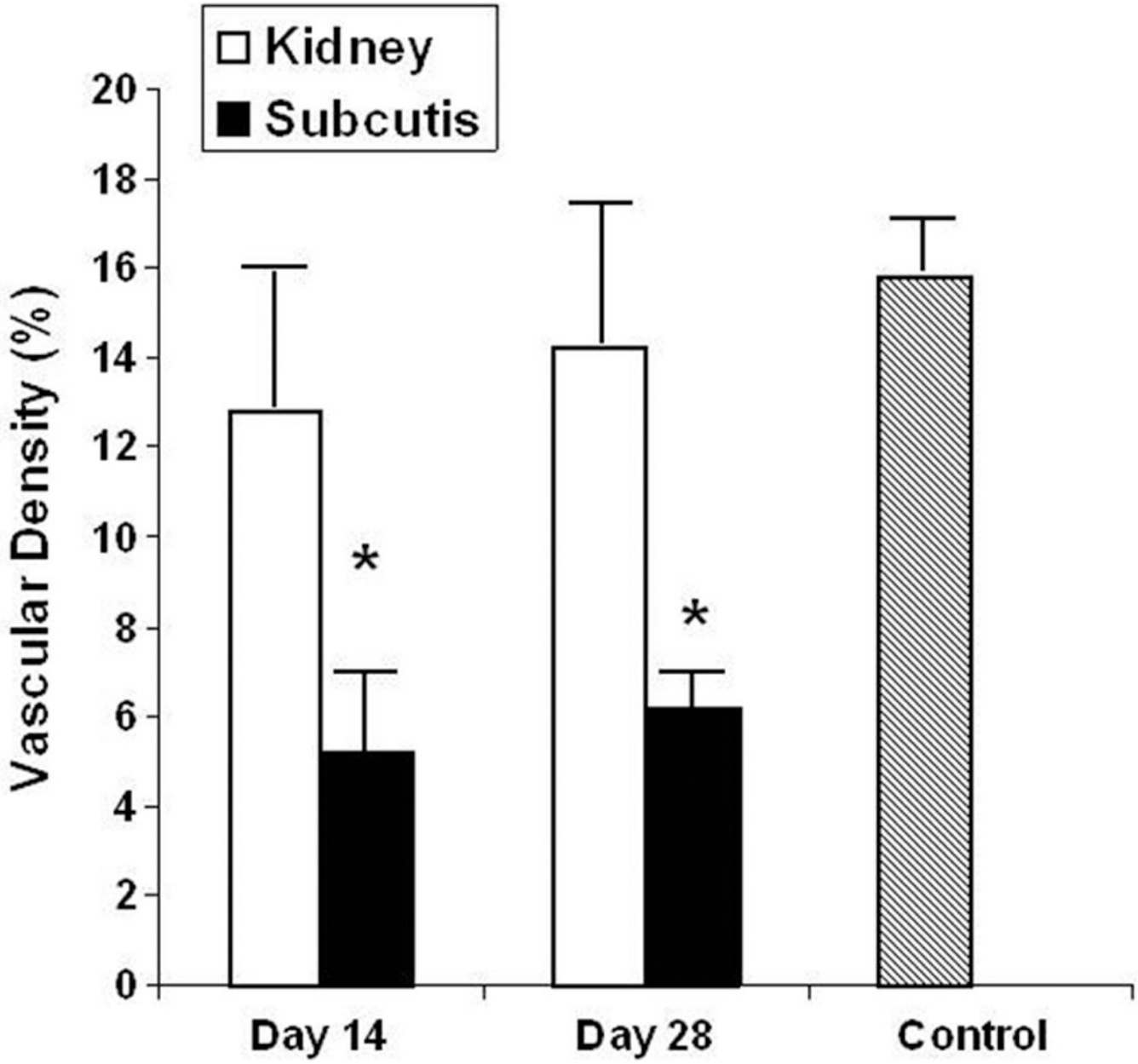

Figure 4. Vascular density

Analysis of areal fraction of CD31-immunoreactive enodothelial cells relative to air-exchanging (septal) parenchyma, expressed as a percentage. Values represent mean ± SD of at least 4 animals per group.

Open bars: kidney grafts; closed bars: subcutaneous grafts; grey bar: control lung (21 weeks' gestation).

*: $P < 0.05$ versus kidney graft.

$watermark-text
$watermark-text
$watermark-text

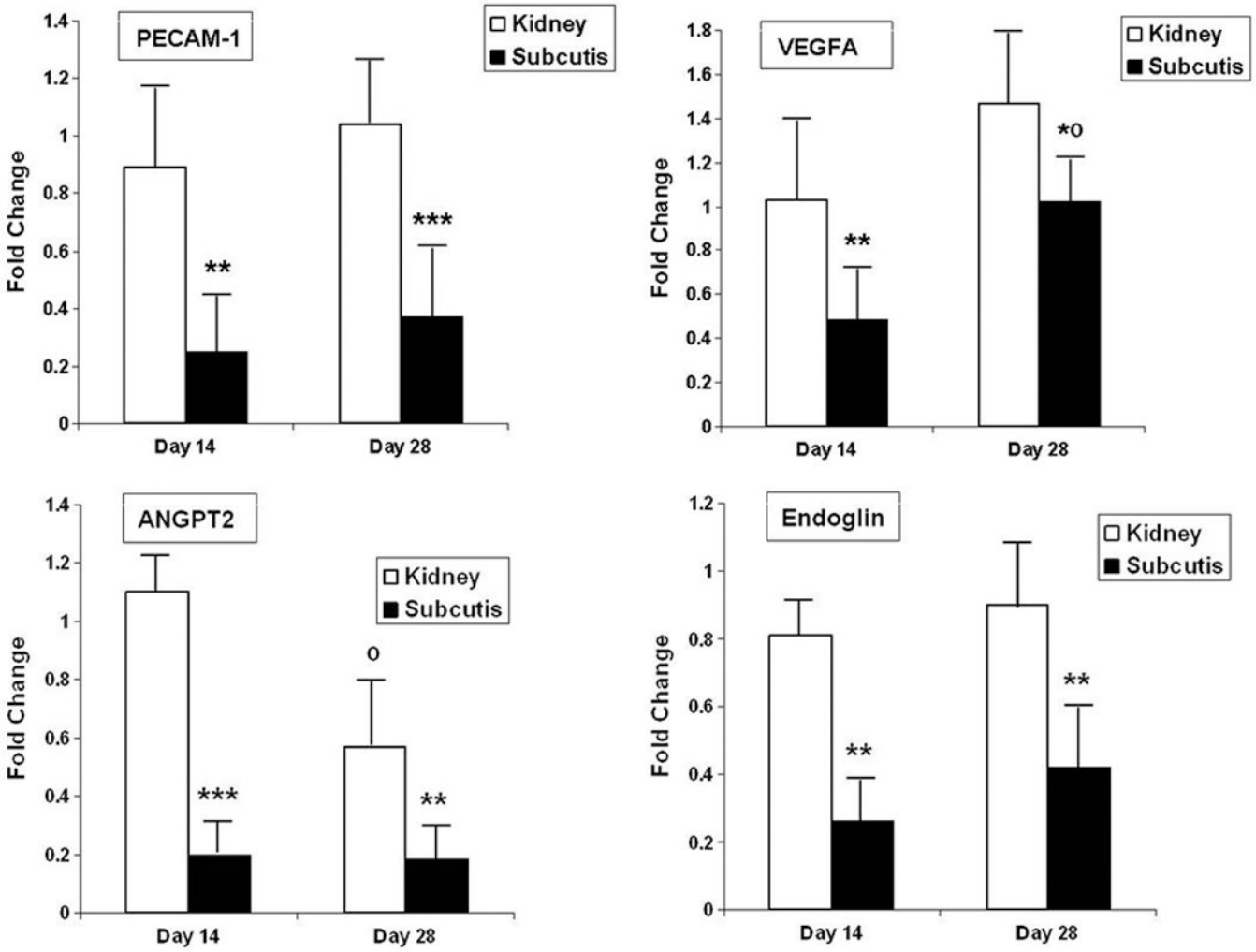

Figure 5. Analysis of angiogenesis-related gene expression

Values represent mean ± SD of 5–6 animals per group, normalized to GAPDH expression. Open bars: kidney grafts; closed bars: subcutaneous grafts.

PECAM-1: platelet endothelial cell adhesion molecule (CD31); VEGFA: vascular endothelial growth cell factor-A; ANGPT2: angiopoietin-2.

*: $P < 0.05$; **: $P < 0.01$; ***: $P < 0.001$ versus kidney graft; º: $P < 0.01$ versus day 14.

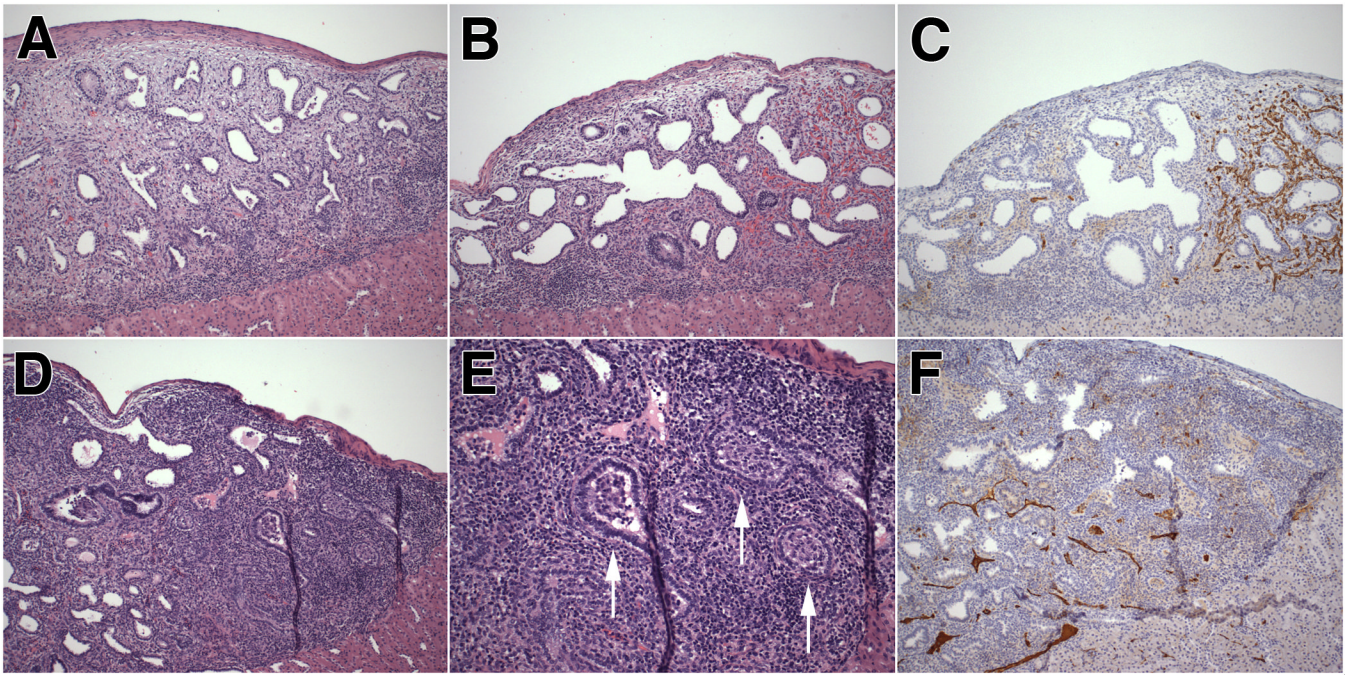

Figure 6. Morphology and vascularization of renal xenograft in the nude rat

A. Representative photomicrograph of renal subcapsular xenograft at post-transplant week 4 showing a band-like inflammatory infiltrate along the graft-kidney border.

B–C. Renal graft at post-transplant week 4 showing prominent inflammation along the graft-kidney interface on the left side of the graft (Fig. 6B), corresponding with decreased vascularization on that side of the graft (Fig. 6C).

D–F. Renal graft at post-transplant week 4 showing dense inflammatory infiltrates deep within the graft. Fibroproliferative plugging of bronchioles is noted, replicating the histopathologic findings of obliterative bronchiolitis in humans (Fig. 6E, arrows). Vascularization is markedly diminished in this severely inflamed graft (Fig. 6F).

A, B, D and E: Hematoxylin-eosin staining; C and F: CD-31 (PECAM-1) immunohistochemical analysis (DAB-peroxidase staining with hematoxylin counterstain). E: original magnification X200; others: original magnification X100.

$watermark-text
$watermark-text
$watermark-text